Electrochimica Acta 483 (2024) 144038

Contents lists available at ScienceDirect

Electrochimica Acta

journal homepage: www.journals.elsevier.com/electrochimica-acta

A Mott-Schottky analysis of mesoporous silicon in aqueous electrolyte solution by electrochemical impedance spectroscopy

Manuel Brinker, Patrick Huber *

Hamburg University of Technology, Institute for Materials and X-ray Physics, Denickestr. 15, 21073, Hamburg, Germany
Centre for X-ray and Nano Science CXNS, Deutsches Elektronen-Synchrotron DESY, 22603, Hamburg, Germany

ARTICLE INFO

Dataset link: https://doi.org/10.15480/882.9268

Keywords:
Nanoporous media
Porous silicon
Electrochemical impedance spectroscopy
Mott-Schottky analysis

ABSTRACT

Nanoporosity in silicon leads to completely new functionalities of this mainstream semiconductor. In recent years, it has been shown that filling the pores with aqueous electrolytes, in addition opens a particularly wide field for modifying and achieving active control of these functionalities, e.g., for electrochemo-mechanical actuation and tunable photonics, or for the design of on-chip supercapacitors. However, a mechanistic understanding of these new features has been hampered by the lack of a detailed characterization of the electrochemical behavior of mesoporous silicon in aqueous electrolytes. Here, the capacitive, potential-controlled charging of the electrical double layer in a mesoporous silicon electrode (pore diameter 7 nm) imbibed with perchloric acid solution is studied by electrochemical impedance spectroscopy. Thorough measurements with detailed explanations of the observed phenomena lead to a comprehensive understanding of the capacitive properties of porous silicon. An analysis based on the Mott-Schottky equation enables the determination of essential parameters such as the flatband potential, the carrier concentration and the width of the space charge region. A comparison with bulk silicon shows that the flatband potential in particular is significantly altered by the introduction of nanopores, as it shifts from 1.4 ± 0.1 V to 1.9 ± 0.2 V.

1. Introduction

Porous silicon is a highly versatile material with a plethora of possible application fields. Porous silicon exhibits outstanding characteristics concerning fundamental properties and combines these in research for applications in a wide variety of research fields. These include medical and biological sciences, where porous silicon has been studied with respect to sensor applications [1–3], optics and electronics [4,5] and a tightly adjustable control of a drug's release kinetics [6]. In fundamental research, porous silicon represents an excellent host material to study the confinement of matter inside the pores, with respect to its structure and dynamics [7–14].

Furthermore, a mechanical actuation in porous silicon induced by humidity or gas sorption has been investigated [15–18]. As a contributing effect of liquid-adsorption measurements, a deformation of porous silicon is revealing porous silicon's mechanics [9,19–21]. A highly reversible deformation, or more precisely straining, of porous silicon in a controlled manner can be achieved either by an electrosorption-induced change in surface stress of the inner surface area of porous silicon [22] or by the incorporation of the electro-active polymer polypyrrole into the pore space of porous silicon [23,24]. These methods have the benefit of operating under electrochemical control and thus the reversible straining is highly adjustable by the applied potential.

Another field of research that employs electrochemical properties of porous silicon is the broad investigation of porous silicon as a lithium battery anode material [25–27].

Porous silicon can be synthesized in an electrochemical etching procedure in hydrofluoric acid. The details of the synthesis have been studied in great detail [28–32]. In particular electrochemical impedance spectroscopy (EIS) has been widely employed to gain a deeper understanding of the electrochemical behavior of porous silicon in hydrofluoric acid solutions and its synthesis process in this electrolyte type [33–38]. Therefore, the focus here is set on an EIS investigation of the electrochemical properties of mesoporous silicon, with a pore diameter of 7 nm (hereafter referred to as simply porous silicon), in another electrolyte type — aqueous acidic solutions. In contact to water, a humid atmosphere or oxygen containing (organic) electrolyte solutions porous silicon is starting to develop a passivating oxide layer right away [31]. To probe the features of pristine silicon, experiments need to be conducted in hydrofluoric acid which immediately removes the oxide layer and hydrates the surface [31]. However, hydrofluoric

* Corresponding author at: Hamburg University of Technology, Institute for Materials and X-ray Physics, Denickestr. 15, 21073, Hamburg, Germany.
E-mail addresses: manuel.brinker@tuhh.de (M. Brinker), patrick.huber@tuhh.de (P. Huber).

https://doi.org/10.1016/j.electacta.2024.144038
Received 7 December 2023; Received in revised form 19 February 2024; Accepted 29 February 2024
Available online 1 March 2024

acid is not an expedient electrolyte for everyday applications, e.g. supercapacitors or sensors in the life sciences, due to its harmful and toxic features. Therefore, the aim of this paper is to explore electrochemical features of porous silicon in a more viable, aqueous electrolyte solution. EIS investigations in aqueous and especially acidic environments focus mostly on an anodic oxidation of porous silicon [39–42]. Rather than that or exploring an electrochemical redox reaction [43], in this publication the reversible charging of the electric double layer (EDL) in a porous silicon electrode is focused.

2. Experimental

Porous silicon is synthesized in an electrochemical anodization procedure. A constant current is applied between a bulk silicon wafer and a platinum counter electrode (CE) in a hydrofluoric acid electrolyte in a PTFE etching cell. The starting material is lightly doped p-type silicon (Si-Mat Silicon Materials GmbH) it has a thickness of 100±10 µm, a (100) orientation and a resistivity of 0.01 − 0.02 Ω cm, which corresponds to a doping level of approximately $3 \cdot 10^{18}$ to $8 \cdot 10^{18}$ cm^{-3} [29]. The current applied accounts to a density of 12.5 mA cm^{-2}. The electrolyte is a 2:3 volumetric mixture of hydrofluoric acid (48%, Merck Emsure) and ethanol (absolute, Merck Emsure). A scanning electron micrograph of the porous silicon layer yields a thickness of 630 nm. A nitrogen sorption isotherm measurement provides an average pore diameter of 3.36 nm and a porosity of 54% for the porous silicon layer. Electrochemically stable porous silicon is needed to perform an EIS analysis. In an acidic aqueous electrolyte solution the porous silicon's inner surface area is oxidized by an applied potential. Therefore, a constant potential of 1.2 V is applied for 24 h. Thus, the oxidative currents are suppressed and solely capacitive currents remain [22]. The procedure is described in more detail in the supplementary information. All in all, the porous silicon electrode has an electrochemically active inner surface area of 164.7 ± 0.4 cm^2. The CE in the EIS experiments consists of a commercially available carbon fabric. It is inert in the electrolyte solution and has a surface are in the range of 1000 m^2.

EIS is performed in a three electrode setup, utilizing a commercial reversible hydrogen reference electrode (RHE, Gaskatel HydroFlex), in an electrolyte solution consisting of 1 mol l^{-1} perchloric acid (70% $HClO_4$, Merck Suprapur, diluted with deionized water). EIS employs an alternating, sinusoidal potential E. It consists of a static potential E_s that stays constant for the duration of the measurement and a sinusoidal potential. The amplitude E_0 of the sinusoidal potential is comparatively small. Here 10 mV are used. The resulting harmonic current response J_s is measured between WE and CE. The potentiostat (Metrohm PGSTAT204) is equipped with an impedance analysis module (Metrohm Autolab FRA32) to perform EIS measurements. The frequency is swept over several decades to perform an EIS analysis. The impedance is recorded and averaged at 12 frequency f steps per decade from 100 kHz down to single Hz. The result is displayed in a Nyquist plot that shows $-Z_{im}$ versus Z_{re}. The aim here is to investigate the EDL charging of the porous silicon electrode. Therefore, the frequency range is chosen accordingly so that in a Nyquist plot a half-circle in the high-frequency range (100 to 1 kHz) and an ensuing vertical increase in the mid-frequency range (1000 to 1 Hz) is resolved.

The evaluation of the porous silicon's capacitive features is conducted in terms of the Mott-Schottky equation [44]

$$c_{SCR}^{-2} = -\frac{2}{eN_a\varepsilon_r\varepsilon_0}\left(E - E_{fb} - \frac{k_B T}{e}\right), \quad (1)$$

where c_{SCR} denotes the capacitance of the space charge region (SCR) on the silicon side of the interface, N_a the semi conductor's carrier concentration, ε_r and ε_0 the relative and vacuum permittivity, respectively. By e, k_B and T is referred to the elementary charge, the Boltzmann constant and the temperature. The Mott-Schottky Eq. (1) conveniently connects the physical property of the SCR capacitance on the one side of the semi-conductor-electrolyte interface to the electrochemical property of applied potential E on the other, solution side of the interface. In a simple experiment, c_{SCR} is measured in dependence of the applied, static potential E_s so that in a plot of c_{SCR}^{-2} versus E_s the slope of the linear relation of the two

$$dc_{SCR}^{-2}/dE_s = -2/eN_a\varepsilon_r\varepsilon_0 \quad (2)$$

yields the carrier concentration N_a [45]. Eq. (2) therefore requires the capacitance normalized to the electrode surface. Furthermore, the sign of the slope indicates the doping type, either n- or p-type [31]. The flatband potential E_{fb} indicates the transition from the depletion regime, where the SCR develops, to the accumulation regime, where the SCR is annihilated by an opposite band bending at the interface. The flatband potential E_{fb} can be determined in the plot of c_{SCR}^{-2} versus E_s by the crossing point with zero, i.e. at $c_{SCR}^{-2} = 0$, where $E = E_{fb} + k_B T/e$. The width w of the SCR is obtained by [46]

$$w = \sqrt{-\frac{2\varepsilon_r\varepsilon_0}{eN_a}(E - E_{fb} - \frac{k_B T}{e})}. \quad (3)$$

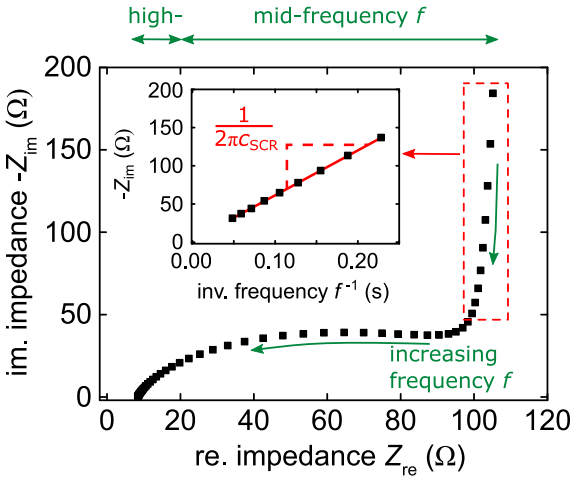

Fig. 1. Characteristic Nyquist plot of a porous silicon electrode in 1 mol l^{-1} perchloric acid at a static applied potential of 0.2 V with frequencies in the range of 100 kHz to 4.3849 Hz. The high-(100 to 1 kHz) and the mid-frequency range (1000 to 4 Hz) are indicated. In the inset the data points of the vertical increase regime at the lowest frequencies (red indication) are plotted versus their inverse frequency f^{-1}. A linear fit to the data points yields a capacitance of c_{SCR} = 0.21 mF.

3. Results & discussion

An exemplary Nyquist plot of a porous silicon electrode in perchloric acid at a static potential of 0.2 V with frequencies in the range of 100 kHz to 4.3849 Hz is depicted in Fig. 1.

The course of the Nyquist plot closely resembles that of a typical EDL charging process in an electrode.

At the highest frequency points, at low values for Z_{re}, the onset of a half-circle can be observed. Subsequently, following an intermediate region, at lower f and larger Z_{re} the data points approach towards a vertical increase. These features are typical for double layer charging [47]. They will be further analyzed in the following.

The intersection at $-Z_{im} = 0$ marks the resistance of the porous silicon electrode [47] and it amounts here to 8.38 Ω. Although the half-circle is not particularly pronounced as compared to other electrodes [47], it can be clearly identified. The diameter of the half-circle determines the bulk electrolytes resistance [47]. It is here 82.1 Ω, which is in good agreement to literature [48]. In the vertical regime following the half-circle, the data points converge to the cut-off frequency at approximately f_c = 4 Hz. The intermediate regime is not distinct, which

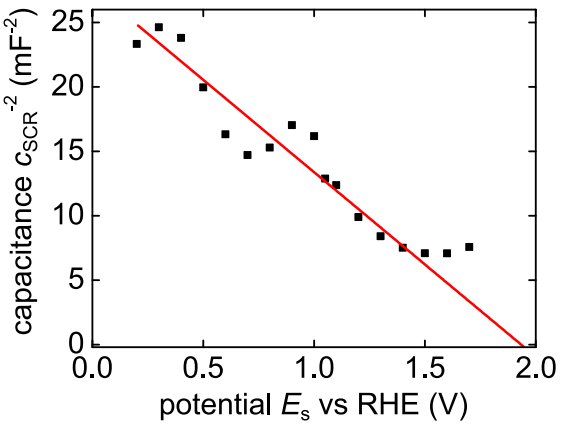

Fig. 2. Mott-Schottky plot of a porous silicon electrode. The capacitance determined by EIS is plotted as c_{SCR}^{-2} versus E_s, the respective static potential. A linear data fit yields a flatband potential of $E_{fb} = 1.9 \pm 0.2$ V and a carrier concentration of $N_a = (3.2 \pm 0.5) \cdot 10^{19}$ cm^{-3}. The linear fit is only performed up until a potential of 1.2 V. The line of the fit is then prolonged to mark the flatband potential at $c_{SCR}^{-2} = 0$.

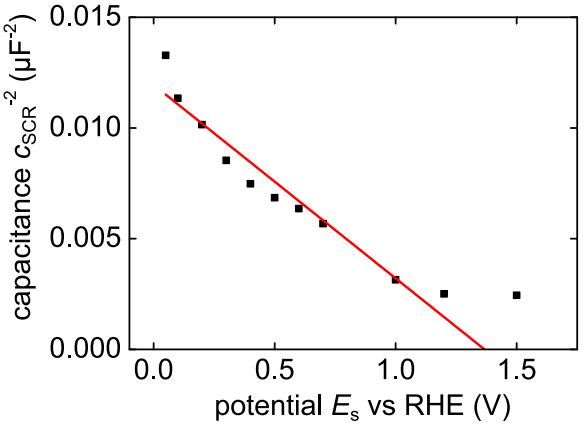

Fig. 3. Mott-Schottky plot of a bulk silicon electrode in 1 mol l^{-1} perchloric acid. The capacitance determined by EIS is plotted as c_{SCR}^{-2} versus the respective static potential E_s. c_{SCR} is determined via EIS measurements with frequencies in the range of 1 MHz to 500 mHz and static potentials in the range of 0.05 – 1.5 V. A linear fit to the Mott-Schottky plot yields a flatband potential of $E_{fb} = 1.4 \pm 0.1$ V and a carrier concentration of $N_a = (2.6 \pm 0.3) \cdot 10^{19}$ cm^{-3}. The linear fit is only performed up until a potential of 1.0 V. The line of the fit is then prolonged to mark the flatband potential at $c_{SCR}^{-2} = 0$.

is an indication that the EDL charging is not inhibited by the resistance of the bulk electrolyte [47].

In the subsequent vertical regime, solely at the lowest frequencies near f_c, the EDL can be considered as fully charged. An approximation by an equivalent circuit of the Nyquist plot's total course constitutes a difficult endeavor as it is often equivocal and prone to errors introduced by choosing an appropriate equivalent circuit [47]. However, in the vertical regime a simple RC-circuit can be utilized to approximate the EDL. The resistance can be identified with Z_{re}, while the capacitance is connected to c_{SCR}. Thus, Z_{im} simplifies to [47]

$$Z_{im} = -\frac{1}{2\pi c_{SCR} f}, \quad \text{for} \quad f < f_c. \tag{4}$$

The data points of the vertical regime near f_c are further analyzed in a second plot, shown in the inset in Fig. 1. Here, $-Z_{im}$ of these points is plotted versus f^{-1}. Their linear dependence is clearly noticeable. The slope of a linear fit to the data is given by $1/2\pi c_{SCR}$. Therefore, it is possible to determine the EDL capacitance as $c_{SCR} = 0.21$ mF. This is in good agreement to a value of 0.26 mF determined by cyclic voltammetry, described in the supplementary information.

The described evaluation procedure for c_{SCR} is repeated for Nyquist plots with different static potentials in the range of $E_s = 0.2$ V – 1.7 V. Thereby, the data for a Mott-Schottky plot is obtained and the result is displayed in Fig. 2. The values for c_{SCR}^{-2} are decreasing with increasing potential E_s. The data points decrease in a linear fashion until an ensuing plateau is reached at approximately 1.4 V and 7 mF^{-2}. However, around 1.0 V the course deviates from the linear dependence and a feature, that could be described as a peak, is present. Surface states occurring on the oxidized surface [49] of the porous silicon electrode would result in such a deviation to higher c_{SCR}^{-2} values [31]. A linear fit to the data in the range up until 1.2 V yields further insights. Firstly, the intersection of the fit with $c_{SCR}^{-2} = 0$ at the abscissa marks the flatband potential. A value of $E_{fb} = 1.9 \pm 0.2$ V is determined. That means, up until E_{fb} the porous silicon electrode is in the depletion regime. This value is larger in comparison to 0.38 V, which marks the flatband potential determined in hydrofluoric acid as an electrolyte solution and for, not porous, but bulk silicon with a resistivity four order of magnitude lower [34]. Porous silicon with a higher conductivity investigated in a non-hydrofluoric aqueous electrolyte might have a higher flatband potential, as seen here [50].

To gain further insight, an equal EIS analysis is performed on bulk silicon. The bulk silicon sample has the same properties as the starting material for the porous silicon synthesis, in particular the same resistivity as stated above. The bulk silicon sample is prepared equally, i.e. the same anodic oxidation step is undertaken. The resulting Nyquist-plots are analyzed in the same fashion as described above so that c_{SCR} is determined for different values of E_s and a Mott-Schottky plot is obtained, depicted in Fig. 3. It has a similar course compared to the Mott-Schottky plot of porous silicon. c_{SCR}^{-2} decreases linearly until a plateau starting at 1.2 V is reached. A linear fit to the data yields a flatband potential of $E_{fb} = 1.4 \pm 0.1$ V. This value is larger in comparison to a value of approximately 0.9 V obtained for bulk silicon with an identical resistivity in an EIS measurement conducted with 1 kHz [51]. However, it has to be noted that this value is obtained in a hydrofluoric acid electrolyte so without any oxide layer. The flatband potential here determined for oxidized bulk silicon is slightly lower in comparison to E_{fb} of oxidized porous silicon. Thus, porous silicon seems to have an altered flatband potential compared to bulk silicon, which has been reported before in literature [33,52]. The values reported before for a porous silicon electrode are lower and in the range of 0.2 V albeit in a hydrofluoric acid electrolyte [33]. Moreover, this flatband potential has been determined on a porous silicon electrode produced from bulk silicon with a three orders of magnitude higher resistivity.

For both the bulk and the porous silicon electrodes a negative slope of the linear fit can be ascertained. Thus, a p-type semiconductor characteristic can be confirmed for the electrodes. Furthermore, the fit's slope yields the carrier concentration, see Eq. (2). A carrier concentration of $N_a = (3.2 \pm 0.5) \cdot 10^{19}$ cm^{-3} is obtained for the porous silicon electrode. The carrier concentration is slightly larger compared to the one stated by the manufacturer, which has been reported before in literature [51]. The fit of the bulk silicon's Mott-Schottky plot yields a carrier concentration of $N_a = (2.6 \pm 0.3) \cdot 10^{19}$ cm^{-3}, which is in good agreement with the porous silicon electrode.

Finally, the knowledge of the flatband potential E_{fb} and the carrier concentration N_a enables a computation of the SCR width within the pore walls of the porous silicon electrode. The boundaries of the applied potential E 0.0 V and 1.2 V lead to width values of $w = 8.9 \pm 0.2$ nm and $w = 5.5 \pm 0.1$ nm. These values seem reasonable as the pore wall thickness is well within this range.

4. Conclusion

In summary, we successfully investigated a porous silicon electrode with respect to a capacitive charging of its electric double layer in an aqueous, non-hydrofluoric electrolyte solution by technique of electrochemical impedance spectroscopy. The Mott-Schottky analysis yields insight into the energetic band structure within the porous silicon pore walls as it was possible to determine the flatband potential and the width of the SCR of the porous silicon electrode. In particular, the flatband potential is significantly altered as it shifts from 1.4 ± 0.1 V to 1.9 ± 0.2 V by the introduction of pores into a silicon electrode.

Overall, this study provides unique insight into the interaction between the semiconductor properties of porous silicon and its electrochemical features. Here, it could be interesting to further investigate porous silicon's potential in terms of a supercapacitor application [53]. A direct measurement of the band bending occurring at the interface, by technique of e.g. photoemission spectroscopy (PES) or scanning tunneling microscopy (STM) might benefit this research area. Furthermore, research into a hybrid material with a deposited metal layer onto the pore walls of porous silicon could benefit from the presented study. The goal to create such a material combination could be to influence the capacitive or conductive features of porous silicon. This hybrid sample type would establish a semiconductor-metal contact at the interface of the pore wall which, in case of a Schottky contact, resembles the electrolyte-semiconductor interface.

CRediT authorship contribution statement

Manuel Brinker: Writing – review & editing, Writing – original draft, Visualization, Validation, Methodology, Investigation, Formal analysis, Data curation, Conceptualization. **Patrick Huber:** Writing – review & editing, Writing – original draft, Validation, Supervision, Formal analysis, Conceptualization.

Declaration of competing interest

The authors declare that they have no known competing financial interests or personal relationships that could have appeared to influence the work reported in this paper.

Data availability

All data that is needed to evaluate the conclusions is presented in the paper. The raw data of the electrochemical impedance spectroscopy experiments is available at TORE (https://tore.tuhh.de/), the Open Research Repository of Hamburg University of Technology, at the doi: https://doi.org/10.15480/882.9268.

Acknowledgments

This work was supported by the Deutsche Forschungsgemeinschaft (DFG), Germany within the Collaborative Research Initiative CRC 986 "Tailor-Made Multi-Scale Materials Systems" Project number 192346071. P.H. also acknowledges support by the CRC 1615 "SMART Reactors for Future Process Engineering" Project number 503850735. This work has also received funding from the European Innovation Council (EIC) under the European Union's Horizon 2020 research and innovation program under grant agreement number 964524 EHAWEDRY: "Energy harvesting via wetting-drying cycles with nanoporous electrodes" (H2020-FETOPEN-1-2021-2025). We also acknowledge the scientific exchange and support of the Centre for Molecular Water Science CMWS, Hamburg (Germany).

Appendix A. Supplementary data

Supplementary material related to this article can be found online at https://doi.org/10.1016/j.electacta.2024.144038.

References

[1] V.S.-Y. Lin, K. Motesharei, K.-P.S. Dancil, M.J. Sailor, M.R. Ghadiri, A porous silicon-based optical interferometric biosensor, Science 278 (5339) (1997) 840–843, http://dx.doi.org/10.1126/science.278.5339.840.
[2] V. Vendamani, S.N. Rao, A.P. Pathak, V.R. Soma, Silicon nanostructures for molecular sensing: A review, ACS Appl. Nano Mater. 5 (4) (2022) 4550–4582, http://dx.doi.org/10.1021/acsanm.1c04569.
[3] M. Sailor, Sensor applications of porous silicon, Properties Porous Silicon 18 (1997) 364–370.
[4] E.C. Wu, J.-H. Park, J. Park, E. Segal, F. Cunin, M.J. Sailor, Oxidation-triggered release of fluorescent molecules or drugs from mesoporous Si microparticles, ACS Nano 2 (11) (2008) 2401–2409, http://dx.doi.org/10.1021/nn800592q.
[5] S. Micera, E. Redolfi Riva, Wireless neuromodulation with porous silicon, Nature Mater. 21 (6) (2022) 614–616, http://dx.doi.org/10.1038/s41563-022-01257-7.
[6] A. Tzur-Balter, Z. Shatsberg, M. Beckerman, E. Segal, N. Artzi, Mechanism of erosion of nanostructured porous silicon drug carriers in neoplastic tissues, Nature Commun. 6 (1) (2015) 1–8, http://dx.doi.org/10.1038/ncomms7208.
[7] S. Gruener, P. Huber, Knudsen diffusion in silicon nanochannels, Phys. Rev. Lett. 100 (6) (2008) 64502, http://dx.doi.org/10.1103/PhysRevLett.100.064502.
[8] S. Calus, D. Rau, P. Huber, A.V. Kityk, S. Całus, D. Rau, P. Huber, A.V. Kityk, S. Calus, Influence of nanoconfinement on the nematic behavior of liquid crystals, Phys. Rev. E 86 (2) (2012) 21701, http://dx.doi.org/10.1103/PhysRevE.86.021701.
[9] G.Y. Gor, L. Bertinetti, N. Bernstein, T. Hofmann, P. Fratzl, P. Huber, Elastic response of mesoporous silicon to capillary pressures in the pores, Appl. Phys. Lett. 106 (2015) 1–13, http://dx.doi.org/10.1063/1.4923240.
[10] D. Kondrashova, A. Lauerer, D. Mehlhorn, H. Jobic, A. Feldhoff, M. Thommes, D. Chakraborty, C. Gommes, J. Zecevic, P. de Jongh, A. Bunde, J. Kärger, R. Valiullin, Scale-dependent diffusion anisotropy in nanoporous silicon, Sci. Rep. 7 (1) (2017) 40207, http://dx.doi.org/10.1038/srep40207.
[11] P. Huber, Soft matter in hard confinement: phase transition thermodynamics, structure, texture, diffusion and flow in nanoporous media, J. Phys.: Condens. Matter 27 (10) (2015) 103102, http://dx.doi.org/10.1088/0953-8984/27/10/103102.
[12] O. Vincent, A. Szenicer, A.D. Stroock, Capillarity-driven flows at the continuum limit, Soft Matter 12 (31) (2016) 6656–6661, http://dx.doi.org/10.1039/C6SM00733C.
[13] L.G. Cencha, G. Dittrich, P. Huber, C.L.A. Berli, R. Urteaga, Precursor film spreading during liquid imbibition in nanoporous photonic crystals, Phys. Rev. Lett. 125 (23) (2020) 234502, http://dx.doi.org/10.1103/PhysRevLett.125.234502.
[14] G. Dittrich, L.G. Cencha, M. Steinhart, R.B. Wehrspohn, C.L.A. Berli, R. Urteaga, P. Huber, Polymeric liquids in mesoporous photonic structures: from precursor film spreading to imbibition dynamics at the nanoscale, J. Chem. Phys. 160 (6) (2024) 064903, http://dx.doi.org/10.1063/5.0189633.
[15] Q. Zhao, J.W.C. Dunlop, X. Qiu, F. Huang, Z. Zhang, J. Heyda, J. Dzubiella, M. Antonietti, J. Yuan, An instant multi-responsive porous polymer actuator driven by solvent molecule sorption, Nature Commun. 5 (1) (2014) 4293, http://dx.doi.org/10.1038/ncomms5293.
[16] C. Ganser, G. Fritz-Popovski, R. Morak, P. Sharifi, B. Marmiroli, B. Sartori, H. Amenitsch, T. Griesser, C. Teichert, O. Paris, Cantilever bending based on humidity-actuated mesoporous silica/silicon bilayers, Beilstein J. Nanotechnol. 7 (1) (2016) 637–644, http://dx.doi.org/10.3762/bjnano.7.56.
[17] P. Fratzl, T. Speck, S. Gorb, Function by internal structure–preface to the special issue on bioinspired hierarchical materials, Bioinspiration Biomim. 11 (6) (2016) 060301, http://dx.doi.org/10.1088/1748-3190/11/6/060301.
[18] G. Dolino, D. Bellet, C. Faivre, Adsorption strains in porous silicon, Phys. Rev. B 54 (24) (1996) 17919–17929, http://dx.doi.org/10.1103/PhysRevB.54.17919.
[19] A. Grosman, J. Puibasset, E. Rolley, Adsorption-induced strain of a nanoscale silicon honeycomb, Europhys. Lett. 109 (5) (2015) 56002, http://dx.doi.org/10.1209/0295-5075/109/56002.
[20] G.Y. Gor, P. Huber, N. Bernstein, Adsorption-induced deformation of nanoporous materials—A review, Appl. Phys. Rev. 4 (1) (2017) 011303, http://dx.doi.org/10.1063/1.4975001.
[21] E. Rolley, N. Garroum, A. Grosman, Using capillary forces to determine the elastic properties of mesoporous materials, Phys. Rev. B 95 (6) (2017) 064106, http://dx.doi.org/10.1103/PhysRevB.95.064106.
[22] M. Brinker, P. Huber, Wafer-scale electroactive nanoporous silicon: Large and fully reversible electrochemo-mechanical actuation in aqueous electrolytes, Adv. Mater. 34 (2022) 2105923, http://dx.doi.org/10.1002/adma.202105923.
[23] M. Brinker, G. Dittrich, C. Richert, P. Lakner, T. Krekeler, T.F. Keller, N. Huber, P. Huber, Giant electrochemical actuation in a nanoporous silicon-polypyrrole hybrid material, Sci. Adv. 6 (40) (2020) eaba1483, http://dx.doi.org/10.1126/sciadv.aba1483.
[24] M. Brinker, P. Huber, Wafer-scale electroactive nanoporous silicon: Large and fully reversible electrochemo-mechanical actuation in aqueous electrolytes, Adv. Mater. 34 (2022) 2105923, http://dx.doi.org/10.1002/adma.202105923.
[25] Z. Jiang, C. Li, S. Hao, K. Zhu, P. Zhang, An easy way for preparing high performance porous silicon powder by acid etching Al–Si alloy powder for lithium ion battery, Electrochim. Acta 115 (2014) 393–398, http://dx.doi.org/10.1016/j.electacta.2013.08.123.

[26] H. Jia, X. Li, J. Song, X. Zhang, L. Luo, Y. He, B. Li, Y. Cai, S. Hu, X. Xiao, C. Wang, K.M. Rosso, R. Yi, R. Patel, J.G. Zhang, Hierarchical porous silicon structures with extraordinary mechanical strength as high-performance lithium-ion battery anodes, Nature Commun. 11 (1) (2020) 1–9, http://dx.doi.org/10.1038/s41467-020-15217-9.

[27] Z. Cheng, H. Jiang, X. Zhang, F. Cheng, M. Wu, H. Zhang, Fundamental understanding and facing challenges in structural design of porous si-based anodes for lithium-ion batteries, Adv. Funct. Mater. 33 (26) (2023) 2301109, http://dx.doi.org/10.1002/adfm.202301109.

[28] L. Canham, Handbook of Porous Silicon, Springer, 2015, http://dx.doi.org/10.1007/978-3-319-71381-6.

[29] V. Lehmann, Electrochemistry of Silicon: Instrumentation, Science, Materials and Applications, Wiley-VCH, Weinheim, 2002, http://dx.doi.org/10.1002/3527600272.

[30] M.J. Sailor, Porous Silicon in Practice - Preparation, Characterization and Applications, Wiley-VCH, Weinheim, 2011.

[31] X.G. Zhang, Electrochemistry of Silicon and Its Oxide, Springer Science & Business Media, 2007, http://dx.doi.org/10.1007/b100331.

[32] X. Cheng, Z.-D. Feng, G.-F. Luo, Effect of potential steps on porous silicon formation, Electrochim. Acta 48 (5) (2003) 497–501, http://dx.doi.org/10.1016/S0013-4686(02)00716-8.

[33] I. Ronga, A. Bsiesy, F. Gaspard, R. Herino, M. Ligeon, F. Muller, A. Halimaoui, Electrical characterization of the silicon-electrolyte interface in the conditions of porous silicon formation, J. Electrochem. Soc. 138 (5) (1991) 1403, http://dx.doi.org/10.1149/1.2085795.

[34] P. Searson, X. Zhang, The potential distribution at the silicon/electrolyte interface in HF solutions, Electrochim. Acta 36 (3–4) (1991) 499–503, http://dx.doi.org/10.1016/0013-4686(91)85133-R.

[35] G. Popkirov, S. Ottow, In situ impedance spectroscopy of silicon electrodes during the first stages of porous silicon formation, J. Electroanal. Soc. 429 (1) (1997) 47–54, http://dx.doi.org/10.1016/S0022-0728(97)00131-9.

[36] V.P. Parkhutik, AC impedance study of porous silicon aging in HF solution, J. Porous Mater. 7 (2000) 97–101, http://dx.doi.org/10.1023/A:1009619415893.

[37] F. Husairi, J. Rouhi, K. Eswar, A. Zainurul, M. Rusop, S. Abdullah, Electrochemical impedance spectroscopy analysis of porous silicon prepared by photo-electrochemical etching: Current density effect, Appl. Phys. A 116 (2014) 2119–2124, http://dx.doi.org/10.1007/s00339-014-8416-1.

[38] A. Mogoda, Y. Ahmad, Electrochemical impedance study of porous silicon prepared by metal-assisted chemical etching, Silicon 11 (2019) 2837–2844, http://dx.doi.org/10.1007/s12633-019-0077-4.

[39] G. Mula, M.V. Tiddia, R. Ruffilli, A. Falqui, S. Palmas, M. Mascia, Electrochemical impedance spectroscopy of oxidized porous silicon, Thin Solid Films 556 (2014) 311–316, http://dx.doi.org/10.1016/j.tsf.2014.01.044.

[40] V. Parkhutik, E. Matveeva, Electrochemical impedance characterization of transient effects in anodic oxidation of silicon, Phys. Status Solidi (a) 182 (1) (2000) 37–44, http://dx.doi.org/10.1002/1521-396X(200011)182:1<37::AID-PSSA37>3.0.CO;2-X.

[41] A. Bsiesy, F. Gaspard, R. Herino, M. Ligeon, F. Muller, J. Oberlin, Anodic oxidation of porous silicon layers formed on lightly p-doped substrates, J. Electrochem. Soc. 138 (11) (1991) 3450–3456, http://dx.doi.org/10.1149/1.2085432.

[42] K.S.A. Cherif, S. Kordic, J. Farkas, S. Szunerits, Electrochemical impedance spectroscopy of dense silica and porous silicon oxycarbide, Electrochem. Solid-State Lett. 10 (9) (2007) G63.

[43] B.-A. Mei, J. Lau, T. Lin, S.H. Tolbert, B.S. Dunn, L. Pilon, Physical interpretations of electrochemical impedance spectroscopy of redox active electrodes for electrical energy storage, J. Phys. Chem. C 122 (43) (2018) 24499–24511, http://dx.doi.org/10.1021/acs.jpcc.8b05241.

[44] N. Sato, Electrochemistry at Metal and Semiconductor Electrodes, Elsevier, 1998, http://dx.doi.org/10.1016/B978-0-444-82806-4.X5000-4.

[45] K. Gelderman, L. Lee, S. Donne, Flat-band potential of a semiconductor: Using the Mott–Schottky equation, J. Chem. Educ. 84 (4) (2007) 685, http://dx.doi.org/10.1021/ed084p685.

[46] M. Grundmann, Physics of semiconductors, vol. 11, Springer, 2010, http://dx.doi.org/10.1007/978-3-319-23880-7.

[47] B.A. Mei, O. Munteshari, J. Lau, B. Dunn, L. Pilon, Physical interpretations of nyquist plots for EDLC electrodes and devices, J. Phys. Chem. C 122 (1) (2018) 194–206, http://dx.doi.org/10.1021/acs.jpcc.7b10582.

[48] L.H. Brickwedde, Properties of aqueous solutions of perchloric acid, J. Res. Natl. Inst. Stand. Technol. 42 (1949) 309–329.

[49] J.-N. Chazalviel, Electrochemical transfer via surface states: A new formulation for the semiconductor/electrolyte interface, J. Electrochem. Soc. 129 (5) (1982) 963, http://dx.doi.org/10.1149/1.2124074.

[50] S. Ottow, G. Popkirov, H. Föll, Determination of flat-band potentials of silicon electrodes in HF by means of AC resistance measurements, J. Electroanal. Soc. 455 (1–2) (1998) 29–37, http://dx.doi.org/10.1016/S0022-0728(98)00189-2.

[51] D. Priyadarshani, P. Leuaa, R. Maurya, A. Kottantharayil, M. Neergat, Semiconductor-to-metal-like behavior of Si with dopant concentration—an electrochemical investigation and illustration with surface hydride formation and hydrogen evolution reaction, J. Phys. Chem. C 124 (37) (2020) 19990–19999, http://dx.doi.org/10.1021/acs.jpcc.0c05616.

[52] S. Merazga, A. Cheriet, K. M'hammedi, A. Mefoued, N. Gabouze, Investigation of porous silicon thin films for electrochemical hydrogen storage, Int. J. Hydrogen Energy 44 (20) (2019) 9994–10002, http://dx.doi.org/10.1016/j.ijhydene.2019.03.017.

[53] A.S. Westover, J.W. Tian, S. Bernath, L. Oakes, R. Edwards, F.N. Shabab, S. Chatterjee, A.V. Anilkumar, C.L. Pint, A.S. Westover, J.W. Tian, S. Bernath, L. Oakes, R. Edwards, F.N. Shabab, S. Chatterjee, A.V. Anilkumar, C.L. Pint, A multifunctional load-bearing solid-state supercapacitor, Nano Lett. 14 (6) (2014) 3197–3202, http://dx.doi.org/10.1021/nl500531r.